Bistatic Polarimetric Measurements and Simulations of a Cessna 172 at DVB-T Frequencies

Idar Norheim-Næss*, Kyrre Strøm*, Erlend Finden*, Øystein Lie-Svendsen*, Terje Johnsen*, Diego Cristallini†, Heiner Kuschel†, Karl Erik Olsen*

*Norwegian Defence Research Establishment, Air and Space Systems Division, P.O. Box 20, NO-2007 Kjeller, NORWAY

†Fraunhofer FHR, Passive Radar and Anti-Jamming Techniques (PSR), Fraunhoferstraβe 20, 53343 Wachtberg-Werthhoven, GERMANY

Idar.Norheim-Nass@ffi.no

ABSTRACT

In June 2016 a field trial was held at Horten in Norway, measuring polarimetric bistatic electromagnetic reflections from a Cessna 172 SP. The transmitter used was Halden Høyås, a 63kW ERP horizontally polarised DVB-T transmitter where the 666 MHz frequency was analysed. The receiver used was Atlantis, a Fraunhofer FHR developed 12 channel passive radar processing and recording system. The surveillance antenna used was produced by the Norwegain Defence Research Establishment (FFI). It is an 11 element dual polarised array antenna, designed as a master's thesis at the Norwegian University of Science and Technology (NTNU) in collaboration with FFI. For the polarimetric measurements the five center elements were used for a total of 10 measured channels, and one separate channel of the Atlantis was used for recording reference data with a Yagi-Uda high-gain antenna. Digital beamforming was used to extract the target data from the resulting range-Doppler matrices separately for the horizontally and vertically polarised arrays, and the resulting measurements were then compared to bistatic polarimetric Radar Cross Section (RCS) simulations at a similar frequency and bistatic geometry. The results indicate that for DVB-T frequencies and horizontally polarised transmitter, a co-polarised surveillance antenna yield a higher Signal-to-Noise ratio (SNR). Results from larger datasets and separate measurement campaigns should however be considered before general recommendations are given.

1.0 INTRODUCTION

Passive radar is well described in [1]. An issue in passive radar is that the strong reference signal from the transmitter and other interference may mask the weaker target echo in the receiver surveillance channel [1]. One technique that reduces this problem is placing nulls in the radiation pattern of the antenna in the direction of the reference signal [2]. Studies have claimed to further reduce this problem in passive radars based on Digital Video Broadcasting-Terrestrial (DVB-T) and Digital Audio Broadcasting (DAB) by applying a cross-polarised receive antenna with respect to the transmitter, arguing that the cross-polarised radar cross section (RCS) is sufficient to give a net increase in signal-to-Noise-Ratio (SNR) [3] [4] [5]. However, if the receiver has enough dynamical range to sample both the weak target signal and the strong reference signal, the problem may be handled digitally. A digital cancellation algorithm or a filter may be applied to reduce the masking effect, and digital beamforming by an antenna array may place nulls in the direction of the transmitter.

Here we study the effect of applying a cross-polarised receiver surveillance antenna. Different polarisation configurations of transmitter and receiver antennas of a frequency modulated (FM)-radio based passive radar have been studied in [6] [7] [8]. It was reported that in some configurations a co-polarised surveillance receive antenna (with respect to the transmitter) gave a higher number of detections while other configurations performed better cross-polarised. However, in the FM-based radar [8] other interference was present in the surveillance channel which could not be removed by the cancellation algorithm. The interference environment is expected to be different for DVB-T than for FM-radio due to the transmission in single frequency networks (SFN). In an SFN the same signal is broadcast from different transmitters in a

geographical area, thus eliminating the problem of other interference at the same frequency. We have not found any publications on studies of DVB-T based polarimetric passive radar in the open literature. It is therefore deemed important to perform an experimental verification of the polarisation state of the target echo. In this paper we present the results from polarimetric measurements of a Cessna 172 SP using a newly developed array antenna, and compare them to electromagnetic simulations of a similar target.

2.0 MEASUREMENT SYSTEM AND CAMPAIGN

2.1 Measurement receiver

The measurement receiver used was the Fraunhofer FHR developed Atlantis DVB-T passive radar sensor and recording system, shown in Fig. 2-1. From top to bottom in the equipment rack are: Two Holzworth 6 and 8 channel synthesizers; three analogue front ends performing amplification, filtration, and a two-stage super-heterodyne tuning to sampling-IF; fan enclosure for A/D cooling; external A/D-converters (developed by Fraunhofer FHR) with FPGA Digital Down-Conversion (DDC) connected pairwise to processing blades by PCI-Express; 8 blade-computers where one is a control server, 6 are processing nodes and one is spare; Online UPS for power backup and filtration.

The receiver system has 12 channels, each capable of approximately 3.5 hours of continuous recording of 32 MHz of bandwidth to disk, which enables offline processing. The system is also capable of real-time processing with digital beamforming, detection and tracking. The receiver is described in detail in [9].

2.2 Surveillance antenna

The dual-polarised array antenna is the result of collaboration between FFI and the Norwegian University of Science and Technology (NTNU). The antenna was designed and measured as a master's thesis in 2014 [10]. The antenna was specified in a frequency range of 622 – 726 MHz, where it would cover mostly two but at least one channel of all the large DVB-T transmitters in the Oslofjord region. The antenna was designed to be a testbed for dual-polarised digital beamforming.

In a project assignment preceding the master's thesis a range of different antenna element designs was explored before deciding on the bowtie design (Fig. 2-2). Simulations were carried out in ANSYS HFSS [11], and several of the promising designs were also measured in an anechoic chamber. The bowtie was also explored in different variations of mechanical bending to widen the opening angle of the element, and differing flare angles of the triangles in the bowtie. A triangular dipole offers wider bandwidth than traditional cylindrical dipoles [12], while maintaining a low cost profile as it can be manufactured as a printed circuit board.

After simulating an 11 element crossed bowtie array antenna with an additional passive terminated element at each end, a prototype 5 element array antenna with reflector was built and measured in an anechoic chamber. The results aligned well with the simulation, only with a resonance frequency offset of about +30 MHz. Based on these results a redesign was done to shift the frequency of the antenna to the desired one, and the resulting simulations of the gain pattern for H- and V-polarisation of the centre element can be seen in Fig. 2-4 and 2-5. The azimuth half power beamwidth is approximately 120° with a maximum realized gain of 6 dB. Also, the polarisation isolation between the H and V bowtie elements is more than 20dB

The array antenna was then built by FFI from the specifications in Table 2-1 (shown in the anechoic chamber in Fig. 2-3), and the design was verified in an anechoic chamber. The results will be presented in October at the 2016 IEEE International Conference on Antenna Measurements & Application Focus on Antenna Systems (2016 IEEE CAMA) in Syracuse, NY, USA.

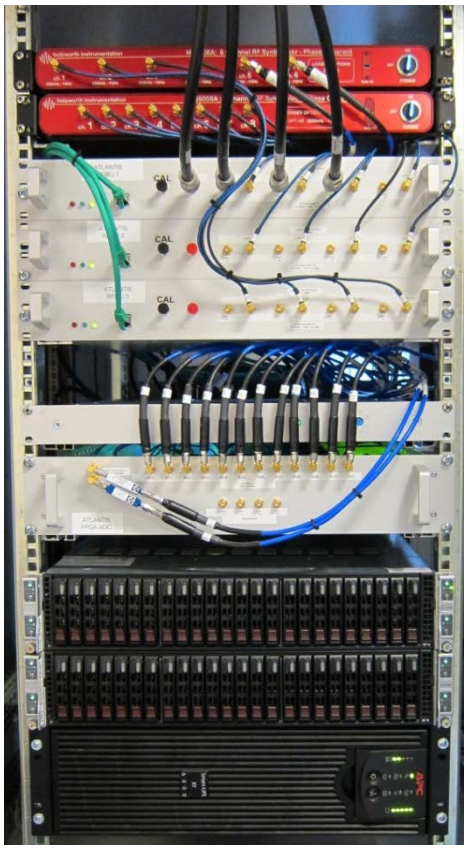

Figure 2-1: Fraunhofer FHR Atlantis DVB-T sensor and recording system (excluding antenna), mounted inside a weather hardened and air-conditioned rack.

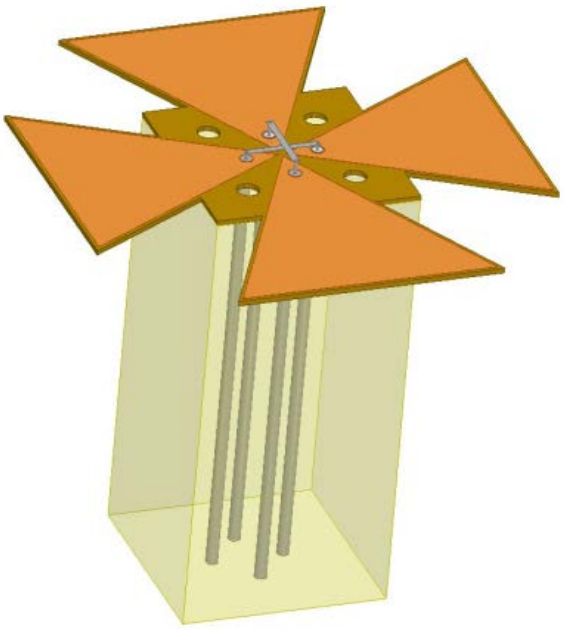

Figure 2-2: Antenna element construction

Figure 2-3: FFI produced and NTNU/FFI designed 11 element dual-polarised antenna based on dual-bowtie elements. One terminated element at each end is added to avoid large differences in the antenna pattern and mutual coupling of the connected elements.

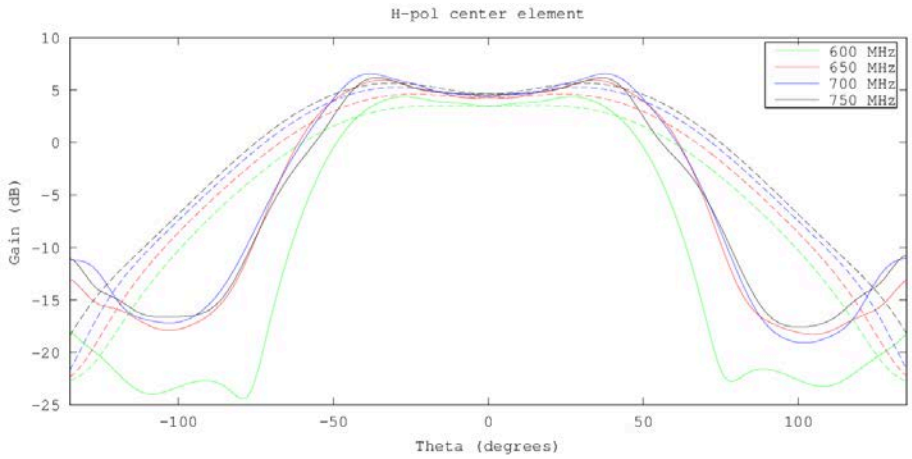

Figure 2-4: Co-polarised response of the H-polarised centre antenna element. Solid lines show the horizontal plane and dotted lines show the vertical plane.

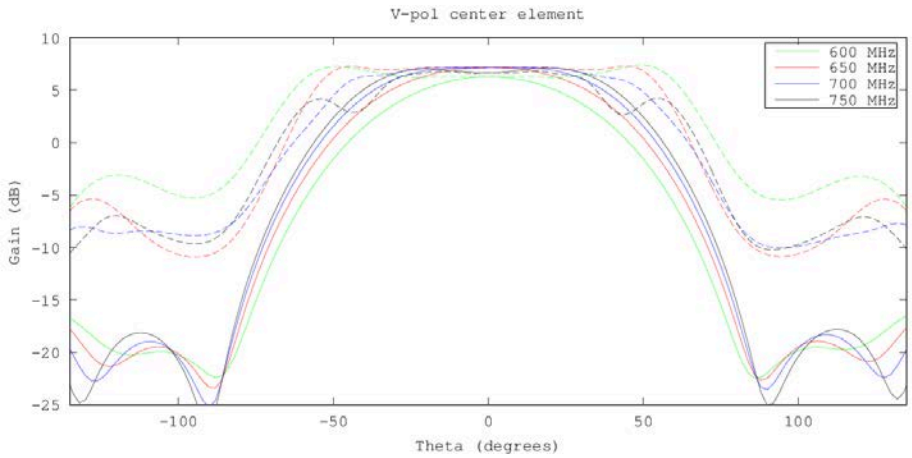

Figure 2-5: Co-polarised response of the V-polarised centre antenna element. Solid lines show the horizontal plane and dotted lines show the vertical plane.

Table 2-1: Geometrical parameters for the bowtie element

Elements	13	Element spacing	260 mm
Balun length	130 mm	Substrate thickness	1.6 mm
Bowtie length (H)	134 mm	Bowtie length (V)	142 mm
Flare angle	56°	Feed gap	2 mm
Ground plane	4 x 0.8 m	Divinycell	60 x 60 mm

2.3 Trial Site and Geometry

The trial site was located at a small peninsula north of Horten in the Oslofjord in Norway. The Atlantis DVB-T Passive Radar sensor system was connected to the surveillance antenna presented in Chapter 2-2, where the 5 centre elements were connected in both H- and V-polarisation for a total of 10 channels. The surveillance antenna was pointing north, with the approximate direction and opening angle shown as a triangle in Fig. 2-6. The 63 kW transmitter used for reference, Halden Høyås, was located at a range of 61 km and a direction of 119° from the receiver (direction shown as green line in Fig. 2-6). A Yagi-Uda antenna of type Televes Dat-HD-75 790 with 19dBi gain was used to receive the reference signal.

2.4 Aircraft and flight pattern

A dedicated flight was performed with a Cessna 172 SP (Reg. LN-FTE) from Tønsberg Flyveklubb, flying at an altitude of 150m above sea level. The partial track that was analysed is shown as a purple line in Fig. 2-6. A timeframe of 5 minutes was analysed and the results are presented in chapter 4.

3.0 BISTATIC DUAL POLARIMETRIC RCS SIMULATIONS

3.1 Calculation Tool and method

The model used for the electromagnetic RCS simulations is shown in Fig. 3.1. The model is based on a commercially bought CAD drawing, adapted for electromagnetic simulations. The coordinate system used throughout the rest of the paper is shown in Fig. 3-1. The aircraft is positioned in the XY-plane with the nose pointing in the negative Y-direction. The usual spherical coordinate system is used, where θ is the angle between the direction vector and the z-axis, and φ the angle between the X-axis and the projection of the direction vector into the XY-plane. Hence $\theta=90^0$, $\varphi=270^0$ gives the forward direction of the aircraft. In the calculations shown here, the illuminator (transmitter) is chosen to be in direction $\theta_i=90°,\varphi_i=225°$, also indicated in Figure 3.1. The aircraft is illuminated with horizontal polarisation at 666 MHz carrier frequency.

RCS calculations have been carried out with a frequency domain electromagnetic solver developed by Efield, now part of ESI [13]. The solver is based on the multilevel fast multipole method (e.g. [14]), which again is based on the method of moments, enabling full-wave calculations of RCS for large, complex structures. The model of the Cessna 172 aircraft is meshed with a triangular mesh width of size 50 mm, corresponding to a tenth of the wavelength at 600 MHz. The surface is treated as one continuous, perfect electric conductor. Hence scattering caused by discontinuities such as door frames and gaps around wing control surfaces are not accounted for.

3.2 Results

Figure 3-2 shows the calculated bistatic RCS in a 90 degree elevation sector centered on the horizontal plane. We note that in a band around the equatorial plane, $\theta=90°$, there is little cross-polarisation. The bottom right panel shows the degree of polarisation of the RCS. Depolarisation should be visible as areas where the ratio between φ-polarised signal and the total RCS would be around 0.5. Near the horizontal plane the RCS is mostly co-polarised (HH). In a 20 degree band centred around the horizontal plane, RCS(HH)>RCS(VH) in 83% of the azimuth/elevation cells, while RCS(HH)>2*RCS(VH) in 71% of the cells. Note also that, in addition to the strong forward scattering, there is strong co-polarised scattering at $\varphi_s=315°$, consistent with specular reflection from the wings, while at ~135° specular reflection from the body of the aircraft is seen.

A “cut” through the RCS at $\theta_s=92°$ degrees is shown in Fig. 3-3. These incident and scattering angles correspond well with the flight of the Cessna shown in Fig. 2-6. We observe again that the RCS is overall higher in H-polarisation than in V-polarisation, in some cases a factor 10-100 higher. In most cases where the co- and cross-polarised RCS are of similar magnitude, the RCS for both are low.

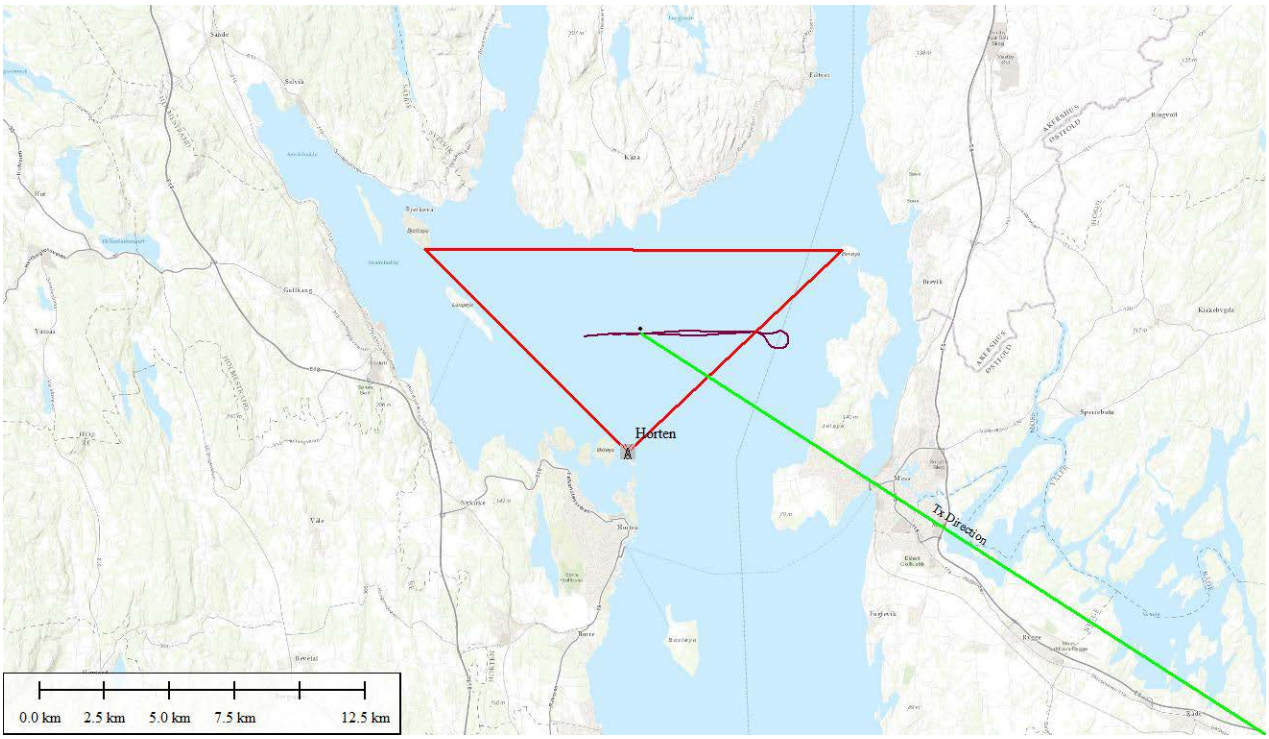

Figure 2-6: Flight pattern flown by the Cessna. Location is about 55km. south of Oslo, Norway. Green solid line show direction to transmitter, red triangle show direction of the surveillance array, and the purple line show the GPS track segment analysed.

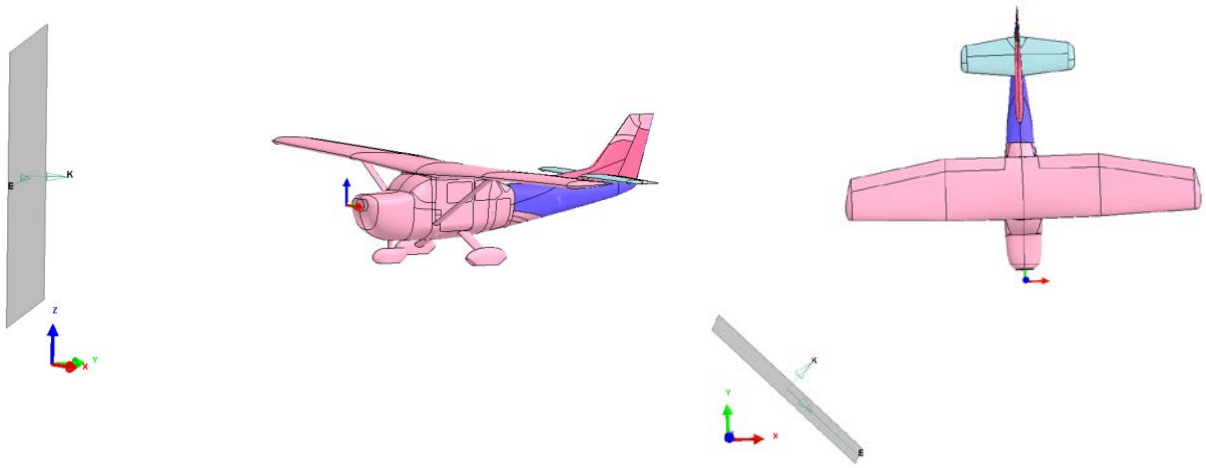

Figure 3.1 Cessna 172 SP model used for RCS calculations (mesh size 50mm). Gray square indicates incoming plane wave with its K-vector. Aircraft is based on a commercial game-model, but adapted for electromagnetic simulations at FFI.

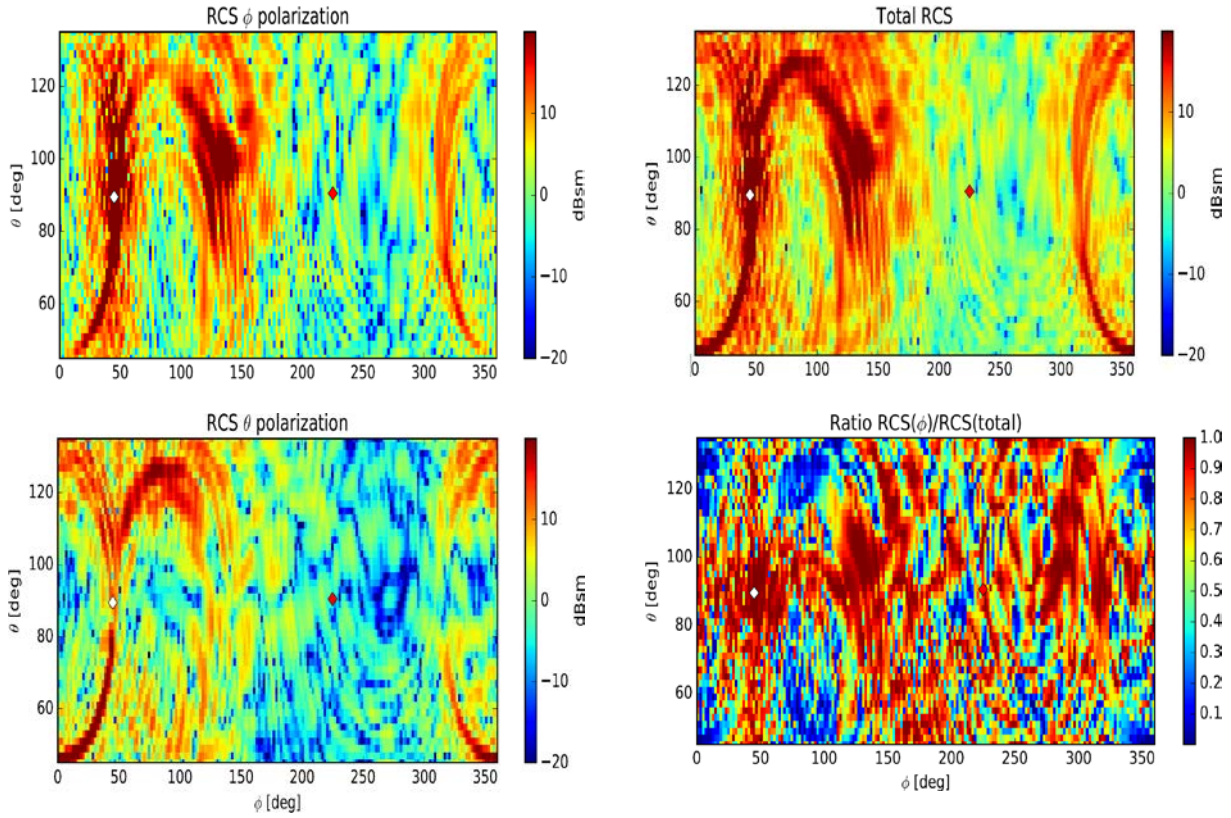

Figure 3-2: RCS simulation of Cessna 172, using a transmitted polarisation along the φ-axis. Top left and bottom left picture shows RCS received with a φ- and θ-polarised antenna respectively. Top right shows the total RCS, and bottom right shows the ratio between φ-polarised RCS and the total RCS. The red diamond marker indicates the direction to the transmitter (illuminator), while the white diamond marker indicates the corresponding forward scattering direction.

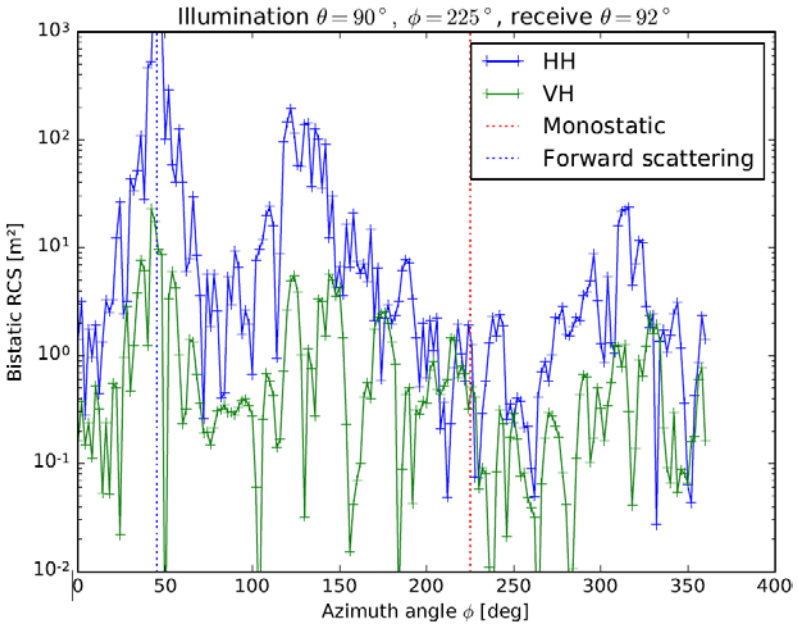

Figure 3-3: A cut through the calculated RCS in Fig. 3-2 at θ_s=92°. The vertical red dotted line indicates the monostatic (backscatter) direction, while the blue dotted line indicates the forward scattering direction.

4.0 COMPARISON OF SIMULATIONS AND MEASUREMENT DATA

The built-in signal processing in the Atlantis sensor was applied as described in [15] to obtain one range-Doppler (RD) map for each receive antenna channel, using a coherent processing interval of 0.52 s. The noise was estimated taking an average of range-Doppler cells at long range and high Doppler frequency, where few aircraft and little clutter is expected to be observed. Digital beamforming with uniform weights was applied, and calculated separately for the H- and V-polarised arrays. An example of a resulting RD-map is shown in Fig. 4-1. We look for detections in a rectangle of the range-Doppler map centred at the global positioning system (GPS)-position of the target. The filtration window used was 7 cells in Doppler and 20 in range (+10 and -9 around the GPS position in range), where Doppler resolution for each cell was 1.938 Hz and range resolution was 32.8 m. The SNR as a function of azimuth scan angle from boresight for H- and V-polarised elements is shown in Fig. 4-2. The peak to sidelobe ratio is approximately 13 dB, as expected for uniform weights. The azimuth direction of the detected target is shown in Fig. 4-3. Detections near 0 Hz Doppler frequency may represent static radar clutter. In Fig. 4-3 and 4-4 markers are placed at clutter detections and at detections where the SNR are below 15 dB.

We observe that the azimuth estimation shown in Fig. 4-4 is coincident with the GPS except for detections in clutter and where the SNR is low, showing that the array is performing well for digital beamforming and direction estimation. The fixed bias of ~5° is probably due to inaccurate array boresight angle given in the beamforming algorithm, as the array direction was estimated manually using a compass. Fig. 4-4 shows SNR. 61% of the time the SNR is more than 3 dB higher using the H-polarised receiver antenna than using the V-polarised, and 74% of the time H-polarised yields higher SNR than V-polarised.

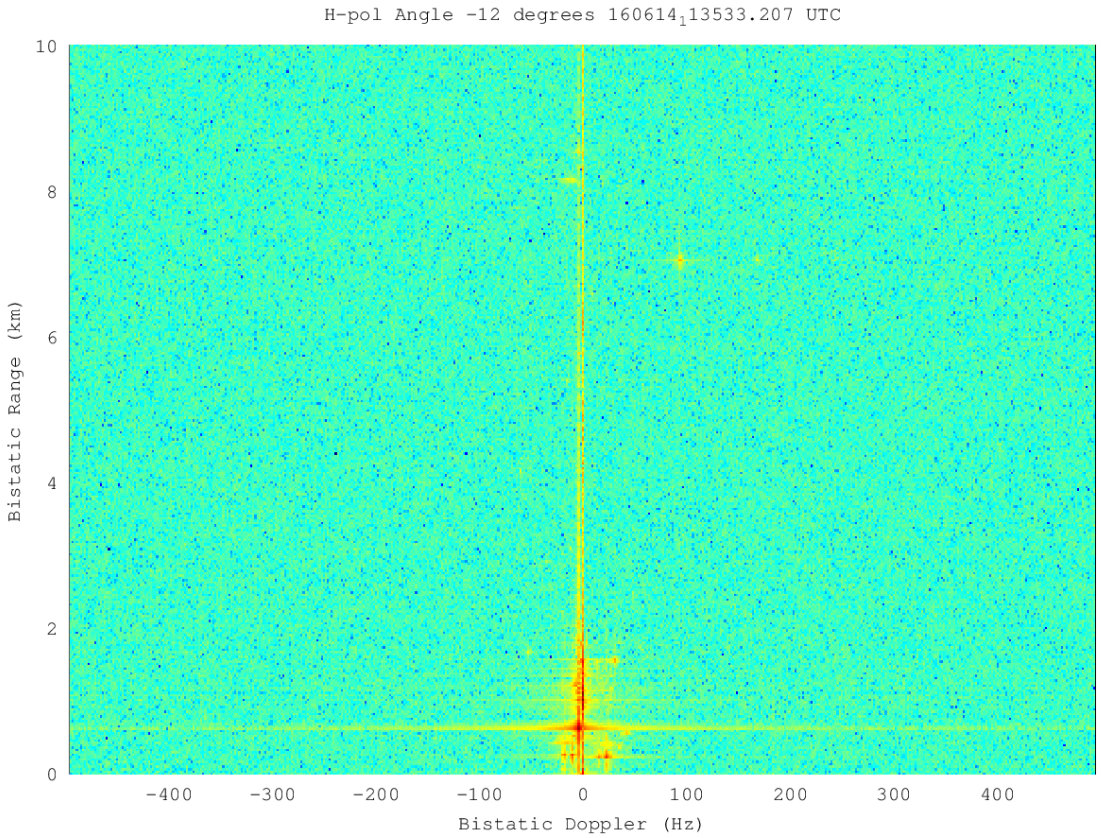

Figure 4-1: Example of range-Doppler map of the H-polarised array after digital beamforming (-12° azimuth). Target is seen at 7 km bistatic range and 100 Hz Doppler. Several boats are visible at close range (0-1 km) and low Doppler.

The applied signal processing [15] is countering the issue of reference signal interference by exploiting orthogonality of the DVB-T signal in a digital filter. In Fig. 4-5 we therefore show both the SNR of the processing scheme with the filter [15] and a scheme without this filter [16]. The filter yields up to 10 dB SNR improvement in H-polarisation where the interference is strong and with no improvement in the V-polarised channel, indicating that there is sufficient dynamical range to handle the interference digitally.

Comparing GPS-tracks to detections in Fig. 4-4, the peaks in H-polarised SNR at 70-110 s and 180-220 s are probably coincident with specular reflection at of the aircraft body, seen at ~315° in Fig. 3-3. Despite the uncertainty in aircraft orientation attitude relative to the GPS velocity vector and the fluctuating nature of RCS, measured ratio of horizontal to vertical SNR agrees qualitatively with the RCS computation.

5.0 CONCLUSION

The array with crossed bowtie elements has proven usable for studies of polarimetric effects of DVB-T based passive radar due to high cross-polarised isolation. The large beamwidth and similar beam pattern of the elements in both H- and V-polarisation allows additional gain and estimation of azimuth by digital beamforming. For the small dataset presented here, in most cases the H-polarised array performed better despite having somewhat lower element gain than the V-polarised elements. Good terrain shielding with the array back-lobe in the direction of the transmitter and a digital filter reduced the reference signal interference in this case. The electromagnetic RCS simulation confirmed that the bistatic RCS was mostly higher in H- than in V-polarisation, given an H-polarised transmitter.

Several independent measurements should be used for more statistics on the subject matter. FFI and Fraunhofer FHR have in September 2016 held a common trial in the same area, but with the addition of an ultra-light aircraft and different bistatic geometry for the FFI sensor. However, the results are not yet finalized. Before recommending in general to use a co-polarised surveillance antenna in DVB-T based passive radar given an H-polarised transmitter network, one should address the following topics: RCS computation and measurement of several target types at several scattering angles, and the ability to reduce reference signal interference (as done in [8]).

ACKNOWLEDGEMENTS

The authors would like to thank Mr. Mathias Tømmer for his work on designing the antenna array, and for re-designing and adjusting the parameters before it could be built and verified in an anechoic chamber by the Norwegian Defence Research Establishment (FFI). We are also grateful for the good advice given by the electronics lab and the workshop of at FFI.

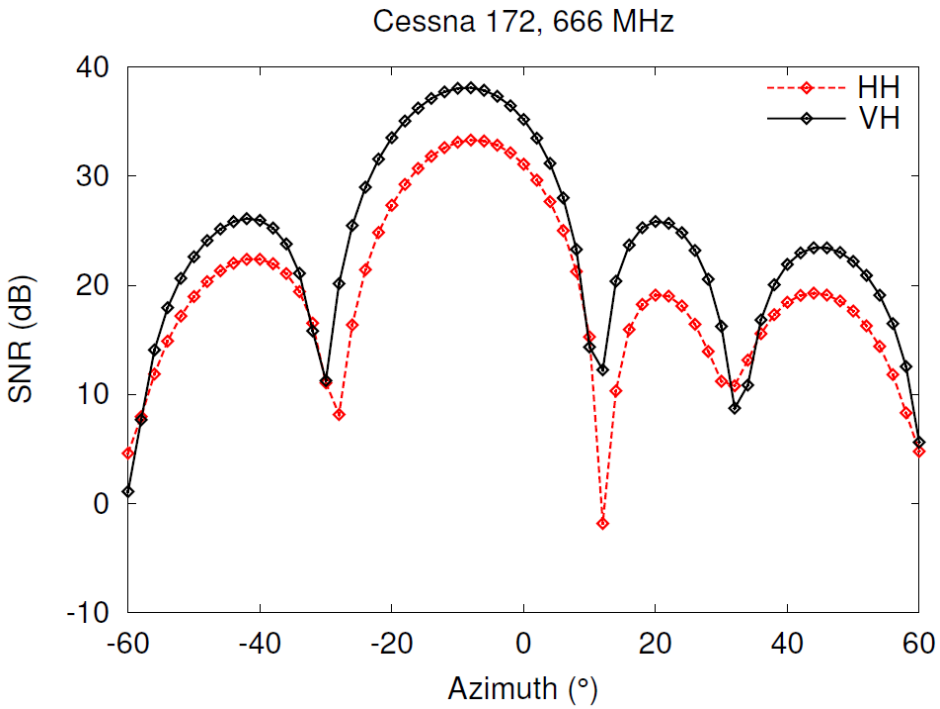

Figure 4-2: The SNR at H-(HH) and V-polarised (VH) receive antennas as a function of azimuth scan angle at time 29 s (Fig. 4-3). The target is located at -10° azimuth.

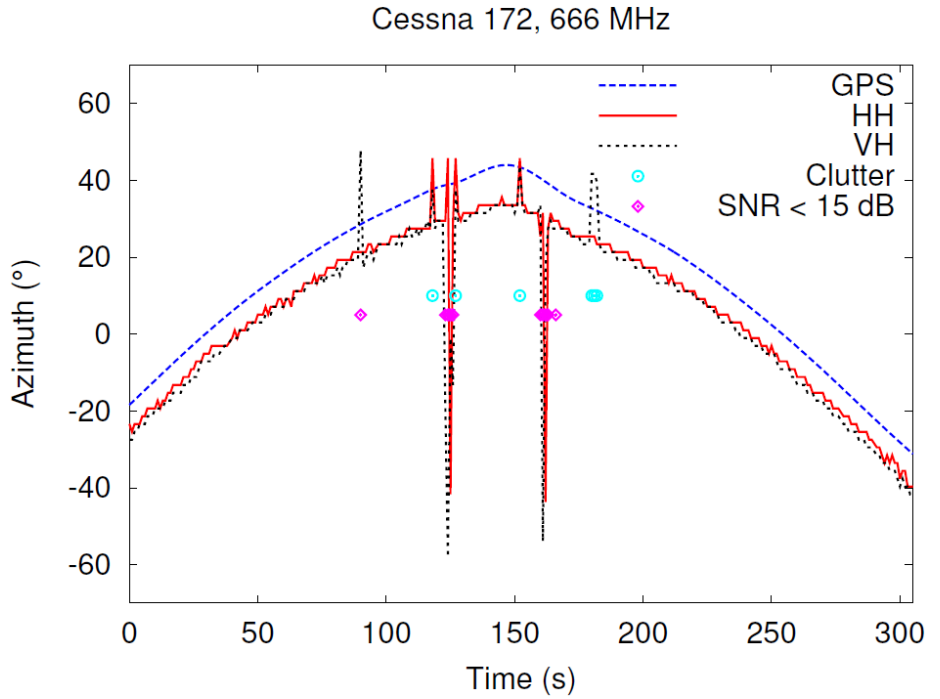

Figure 4-3: Detections in azimuth as a function of time for H-(HH) and V-polarised (VH) receive antennas shown with the azimuth obtained from the GPS-track. Offset between GPS track and antenna direction estimation is caused by manual alignment of antenna. Also indicated are detections with SNR lower than 15 dB and detections near clutter at 0 Hz Doppler frequency.

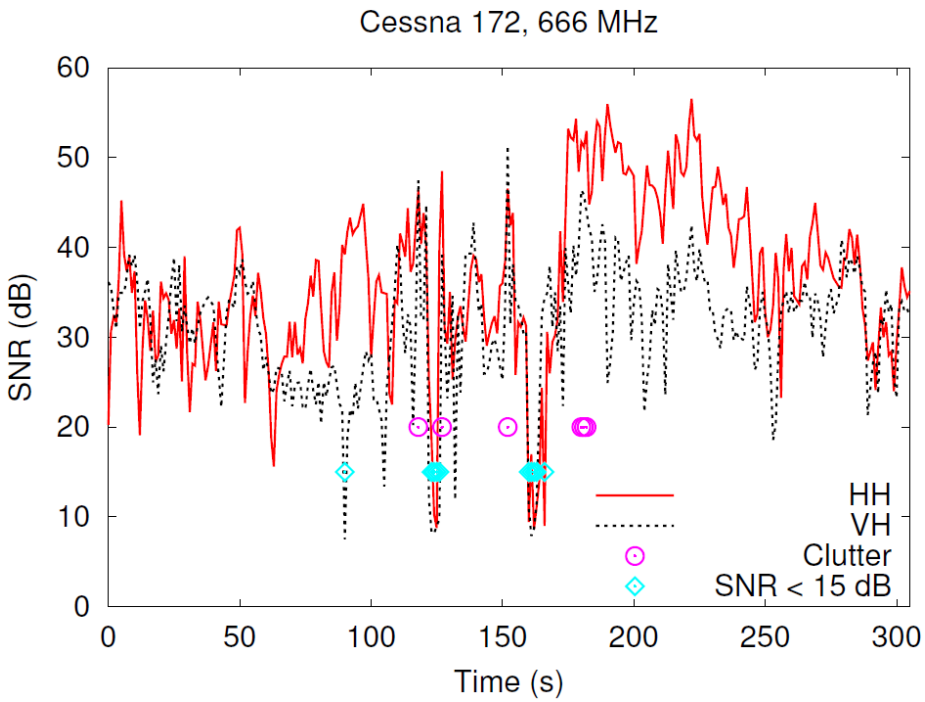

Figure 4-4: Detections of the Cessna 172 with H-polarised (HH) and V-polarised (VH) receive antennas. Also indicated are detections with SNR lower than 15 dB and detections near clutter at 0 Hz Doppler frequency.

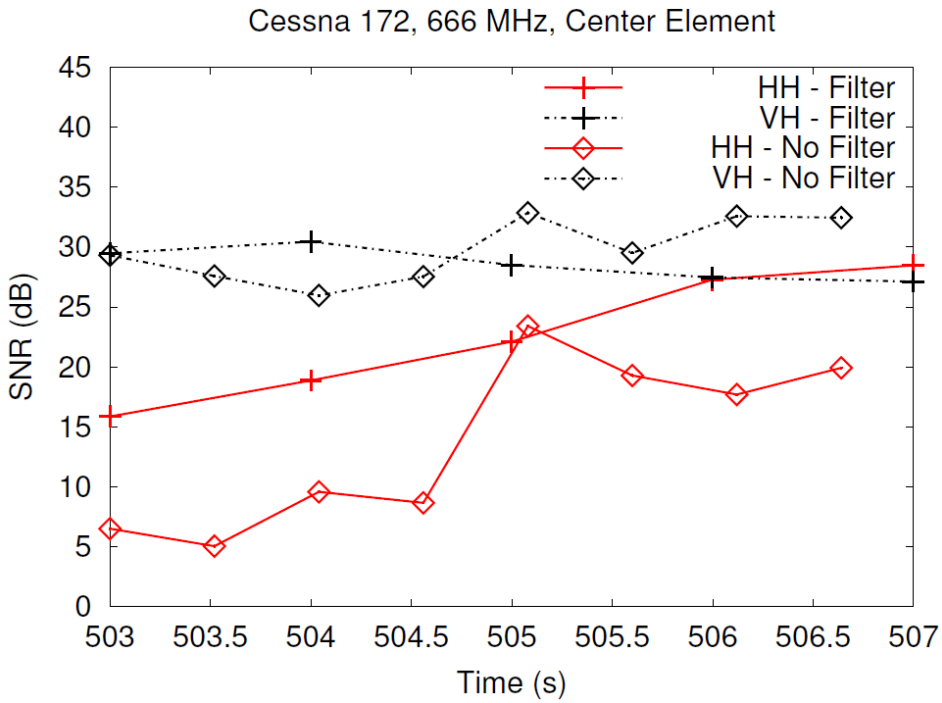

Figure 4-5: The SNR as a function of time measured with a single H-(HH) and a single V-polarised (VH) receive antenna. Two signal processing schemes are shown.

REFERENCES

[1] P. E. Howland, H. D. Griffiths and C. J. Baker, Passive Bistatic Radar Systems: Emerging Technology, M. Cherniakov, Ed., West Sussex: Wiley, 2008, pp. 247-313.

[2] H. D. Griffiths and N. R. W. Long, "Television-based bistatic radar," in *IEE Proceedings F - Communications, Radar and Signal Processing*, Dec. 1986.

[3] R. Saini, M. Cherniakov and V. Lenive, "Direct path interference suppression in bistatic system: DTV based radar," *Radar Conference 2003, Proceedings of the International IEEE,* pp. 309-314, 2003.

[4] C. Coleman and H. Yardley, "Passive bistatic radar based on target illuminations by Digital Audio Broadcasting," *Radar, Sonar & Navigation, IET,* vol. 2, no. 5, pp. 366-375, 2008.

[5] C. Coleman, R. Watson and H. Yardley, "A practical bistatic passive radar system for use with DAB and DRM illuminators," in *Proc. 2008 IEEE Radar Conference*, Rome, 2008.

[6] C. Bongioanni, F. Colone, T. Martelli, R. D'Angeli and P. Lombardo, "Exploiting polarimetric diversity to mitigate the effect of interferences in FM-based passive radar," *11-th International Radar Symposium 2010,* pp. 1-4, 2010.

[7] F. Colone and P. Lombardo, "Exploiting polarimetric diversity in FM-based PCL," *2014 International Radar Conference IEEE,* vol. 51, pp. 1-6, 2014.

[8] F. Colone and P. Lombardo, "Polarimetric passive coherent location," *Aerospace and Electronic Systems, IEEE Transactions on,* vol. 51, pp. 1079-1097, 2015.

[9] J. Schell, J. Heckenbach and H. Kuschel, "ATLANTIS, a scalable, modular PCL receiver for OFDM signals," in *NATO SET-187 Specialist Meeting on Passive Radar, challenges concerning theory and practice in military application*, Szczecin, Poland, 13-14.05.2013.

[10] M. Tømmer, "Design of a phased array antenna for a DVB-T based passive bistatic radar," Norwegian University of Technology and Science (NTNU), Trondheim, Norway, 2014.

[11] ANSYS, "HFSS," ANSYS, [Online]. Available: http://www.ansys.com/Products/Electronics/ANSYS-HFSS. [Accessed 27 09 2016].

[12] G. H. Brown and O. M. Woodward Jr., "Experimentally determined radiation characteristics of conical and triangular antennas," *RCA Review,* vol. 13, pp. 425-452, 1952.

[13] ESI Group, "Computational Electromagnetic (CEM) Solution for Full Virtual Testing," ESI Group, [Online]. Available: https://www.esi-group.com/software-solutions/virtual-environment/electromagnetics. [Accessed 27 09 2016].

[14] J. Song, C. Lu and W. C. Chew, "Multilevel fast multipole algorithm for electromagnetic scattering by large complex objects," *IEEE Transactions on Antennas and Propagation,* vol. 45, no. 10, pp. 1488-1493, 1997.

[15] S. Searle, J. Palmer, L. Davis, D. O'Hagan and M. Ummenhofer, "Evaluation of the Ambiguity Function for Passive Radar with OFDM Transmissions," in *2014 IEEE Radar Conference*, Cincinnati, OH, USA, 2014.

[16] P. Lombardo and F. Colone, Advanced Processing Methods for Passive Bistatic Radar Systems, W. L. Melwin and J. A. Scheer, Eds., Edison, NJ: Scitech Publishing, 2013, p. 751.